Title
Mechanism of IAPP amyloid fibril formation involves an intermediate with a transient β-sheet

Journal
Proceedings of the National Academy of Sciences of the United States of America, 110(48)

ISSN
0027-8424

Authors
Buchanan, Lauren E
Dunkelberger, Emily B
Tran, Huong Q
et al.

Publication Date
2013-11-26

DOI
10.1073/pnas.1314481110

Peer reviewed

Mechanism of IAPP amyloid fibril formation involves an intermediate with a transient β-sheet

Lauren E. Buchanan[a], Emily B. Dunkelberger[a], Huong Q. Tran[a], Pin-Nan Cheng[b], Chi-Cheng Chiu[c,d], Ping Cao[e], Daniel P. Raleigh[e], Juan J. de Pablo[c,d], James S. Nowick[b], and Martin T. Zanni[a,1]

[a]Department of Chemistry, University of Wisconsin–Madison, Madison, WI 53706-1396; [b]Department of Chemistry, University of California, Irvine, CA 92697-2025; [c]Institute for Molecular Engineering, The University of Chicago, Chicago, IL 60637; [d]Argonne National Laboratory, Lemont, IL 60439; and [e]Department of Chemistry, State University of New York, Stony Brook, NY 11794-3400

Edited by Robert Tycko, National Institutes of Health, Bethesda, MD, and accepted by the Editorial Board October 15, 2013 (received for review August 1, 2013)

Amyloid formation is implicated in more than 20 human diseases, yet the mechanism by which fibrils form is not well understood. We use 2D infrared spectroscopy and isotope labeling to monitor the kinetics of fibril formation by human islet amyloid polypeptide (hIAPP or amylin) that is associated with type 2 diabetes. We find that an oligomeric intermediate forms during the lag phase with parallel β-sheet structure in a region that is ultimately a partially disordered loop in the fibril. We confirm the presence of this intermediate, using a set of homologous macrocyclic peptides designed to recognize β-sheets. Mutations and molecular dynamics simulations indicate that the intermediate is on pathway. Disrupting the oligomeric β-sheet to form the partially disordered loop of the fibrils creates a free energy barrier that is the origin of the lag phase during aggregation. These results help rationalize a wide range of previous fragment and mutation studies including mutations in other species that prevent the formation of amyloid plaques.

inhibitors | aggregation pathway | vibrational coupling

The misfolding of proteins into β–sheet-rich amyloid fibrils is associated with the pathology of more than 20 human diseases, including Alzheimer's, Parkinson, and Huntington diseases (1). Amyloid plaques are formed by masses of fibrils, but growing evidence suggests that the toxic species may be prefibrillar intermediates (2, 3). As a result, there is much interest in understanding the mechanism by which these proteins form fibrils and identifying intermediates in the aggregation pathway. However, obtaining structural information about intermediate species is difficult due to their transient nature. Solid-state NMR (ssNMR) and X-ray crystallography provide high-resolution structures of fibrils (4, 5) and optical techniques can track structural changes in real time (6, 7), but few techniques have both the structural and the temporal resolution to extract specific structural details about intermediates. Fragments have been trapped in intriguing oligomeric structures that may represent intermediate states (5, 8) and transient secondary structures are known to exist from circular dichroism measurements and other experiments (9–11), but for full-length proteins it has been difficult to identify the specific residues that contribute to the secondary structure and thus understand their role in the aggregation mechanism. In this paper, we use 2D infrared (2D IR) spectroscopy and isotope labeling to monitor the structural evolution of the full-length human islet amyloid polypeptide (hIAPP or amylin), a 37-residue peptide implicated in type 2 diabetes. We observe the formation of a structured prefibrillar intermediate in a region that has long been known to influence aggregation, but that does not form well-ordered cross-β structure in the amyloid fibril. Its presence provides unique structural insights into the mechanism of amyloid aggregation and helps unify many seemingly inconsistent prior studies.

Many studies on hIAPP have focused on the region spanning residues 20–29 because it plays a critical role in fibril formation. Amyloid fibrils are found only in humans, cats, and some primates (12) even though the sequence for all mammals is highly conserved except for residues 20–29 (Fig. S1*A*). Early work revealed a correlation between the ability to form amyloid in vitro and the sequence in the 20–29 region (13, 14). The fragment $hIAPP_{20–29}$ (SNNFGAILSS) readily forms amyloid fibrils, as do smaller fragments such as $hIAPP_{23–27}$ (13–17) and $hIAPP_{21–27}$; the latter has been characterized with X-ray crystallography (5). Molecular dynamics simulations corroborate the assembly of such fragments into β-sheet structures (18–20). Although other segments also form amyloid fibrils (21, 22), the simplest explanation for the correlation between the sequence and propensity for fibril formation is that the region near 20–29 forms β-sheets that are the "amyloidogenic core" of the fibrils (14, 15, 17, 23). This hypothesis is also consistent with many single-point mutations within residues 20–29 of hIAPP that can decrease or prevent fibril formation (23–25). However, this long-standing hypothesis was recently discredited by ssNMR, which showed that the majority of the residues attributed to the amyloidogenic core did not form β-sheets in the fibril, but instead created a partially disordered loop (Fig. 1 *A* and *B*) (4). A loop should be able to accommodate many types of mutations, making it unclear why this region has such a dramatic impact on aggregation. The results presented here reveal an intermediate with parallel β-sheet structure spanning residues 23–27 that is ultimately disrupted to form the loop of the fibril. The location of this transient β-sheet explains the importance of the FGAIL region in the aggregation of hIAPP and provides a structural explanation for the lag phase that is a unifying feature of all amyloid proteins.

Significance

There is an enormous interest in the mechanism by which proteins misfold and aggregate into amyloid fibrils. Amyloid has been implicated in many human diseases, but the mechanism of aggregation is not understood. Intermediates have been postulated to play an important role in the process, but there have been very few direct measurements that provide specific structural details. The use of isotope labeling and 2D IR methods has allowed the characterization of a critical intermediate generated during amyloid formation by islet amyloid polypeptide, the peptide responsible for amyloid formation in type 2 diabetes. Identification of this intermediate provides a structural explanation for the lag phase and may explain why some species develop amyloid deposits of hIAPP while others do not.

Author contributions: L.E.B., E.B.D., D.P.R., J.J.d.P., J.S.N., and M.T.Z. designed research; L.E.B., E.B.D., H.Q.T., P.-N.C., C.-C.C., and P.C. performed research; L.E.B., E.B.D., H.Q.T., and C.-C.C. analyzed data; and L.E.B. and M.T.Z. wrote the paper.

The authors declare no conflict of interest.

This article is a PNAS Direct Submission. R.T. is a guest editor invited by the Editorial Board.

[1]To whom correspondence should be addressed. E-mail: zanni@chem.wisc.edu.

This article contains supporting information online at www.pnas.org/lookup/suppl/doi:10.1073/pnas.1314481110/-/DCSupplemental.

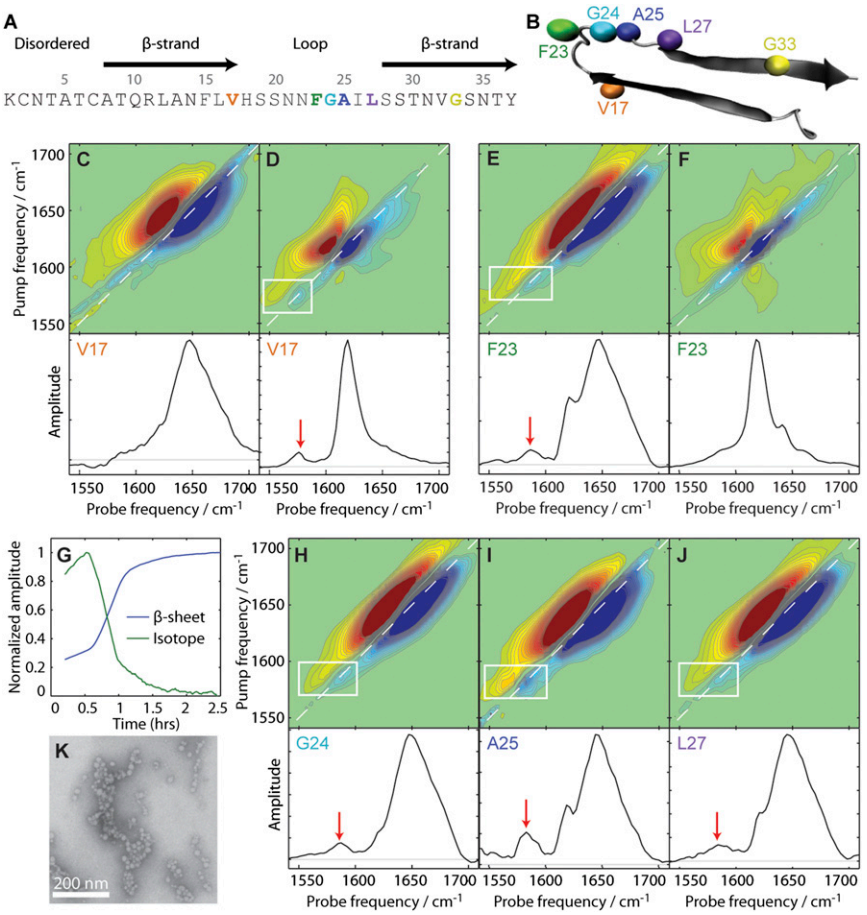

Fig. 1. Structure, 2D IR data, and TEM of isotope-labeled hIAPP. (*A* and *B*) Sequence (*A*) and ssNMR model (*B*) (4) of hIAPP fibrils. β-Sheets are marked with black arrows and isotope-labeled positions with beads. (*C*–*F*) Two-dimensional IR spectra and diagonal intensity slices of lag-phase and equilibrated-phase V17 (*C* and *D*) and F23 (*E* and *F*), respectively. (*G*) Kinetics of the unlabeled β-sheet (1,620 cm^{-1}, blue) and isotope-labeled modes (1,587 cm^{-1}, green) for F23. (*H*–*J*) Lag-phase spectra and slices for G24 (*H*), A25 (*I*), and L27 (*J*). Coupled isotope-labeled modes are highlighted with a white box and a red arrow. (*K*) Electron micrograph of lag-phase hIAPP. (Scale bar, 200 nm.)

Results

The FGAIL Region Forms β-Sheets in a Lag-Phase Oligomer. Using rapid-scan 2D IR spectroscopy, we follow the structural changes of hIAPP aggregation by monitoring the frequency of the amide I band created by backbone carbonyl stretches: Random coil structures absorb near 1,645 cm^{-1}, whereas amyloid β-sheets absorb near 1,620 cm^{-1}. The time course of amyloid aggregation, obtained by monitoring the β-sheet mode at 1,620 cm^{-1}, follows a sigmoidal curve consisting of a lag phase, a growth phase, and an equilibrated phase in which the complete fibril structure has formed (for example, Fig. 2). This growth curve is similar to that obtained using thioflavin-T fluorescence assays (Fig. S2). Residue-level structural resolution is achieved by isotope labeling a single backbone carbonyl with $^{13}C = {}^{18}O$, which spectroscopically resolves the labeled residue from the "bulk" unlabeled modes. In a random coil conformation, isotope-labeled residues typically absorb at 1,595 cm^{-1}. Within an in-register parallel β-sheet conformation, the labeled residues form a coupled linear chain along the length of the sheet, shifting the isotope mode frequency to between 1,570 cm^{-1} and 1,588 cm^{-1}, depending on the precise coupling strength and structural order of the labeled residue. Isotope dilution experiments, in which only 25% of the peptides are labeled, provide an independent test of β-sheet structure by eliminating the effects of coupling and its characteristic spectral shift without changing the structure (26, 27). This labeling strategy has previously been used to study amyloid structure, aggregation kinetics, and inhibitor binding (26, 28, 29).

Samples of 0.5 mM hIAPP labeled with $^{13}C = {}^{18}O$ at residues V17, F23, G24, A25, L27, and G33 were studied (Fig. 1 *A* and *B*). Shown in Fig. 1 *C* and *D* are 2D IR spectra and diagonal slices of the V17-labeled peptide obtained during the lag phase and the equilibrated phase, respectively. In Fig. 1*C*, the pair of broad peaks centered around 1,645 cm^{-1} is the signature of a disordered peptide. The V17 isotope label appears at 1,595 cm^{-1} and is very weak and broad, indicating it is also in a random coil confirmation. The spectrum of the final fibrils (Fig. 1*D*) displays a pair of sharp peaks at 1,620 cm^{-1}, which are characteristic features of amyloid β-sheets formed by the unlabeled residues. Likewise, we know that the V17 residue is incorporated into a parallel β-sheet in the fibril because it exhibits a peak at 1,578 cm^{-1} (Fig. 1*D*, box and arrow), which we verify with isotope dilution (Fig. S3*A*). Thus, V17 has gone from a disordered to a β-sheet structure upon fibril formation, as expected because V17 resides in a well-ordered region of the N-terminal β-sheet according to the ssNMR structure (4, 30).

Spectra obtained for the F23-labeled peptide are markedly different. The lag-phase spectrum (Fig. 1*E*) has the broad peaks at 1,645 cm^{-1} expected for a random coil, but the F23 label exhibits a sharp peak at 1,587 cm^{-1} (box and arrow), indicative of parallel β-sheet formation. β-sheet structure is confirmed by dilution experiments (Fig. S3*B*). Thus, during the lag phase, most residues are disordered whereas F23 participates in a parallel β-sheet. In the equilibrated fibril, the label absorbs at 1,593 cm^{-1} and is weak and broad (Fig. 1*F*), consistent with the ssNMR model (4) in which F23 resides within the partially ordered loop of the fibril where the coupling is overwhelmed by the structural disorder. The evolution of a sharp peak to a weak and broad feature, indicating a local structural change from a parallel β-sheet to a more disordered structure, is the opposite of what was observed for V17.

Monomeric hIAPP cannot produce the coupling necessary to generate the peak at 1,587 cm^{-1}; only the presence of an aggregated

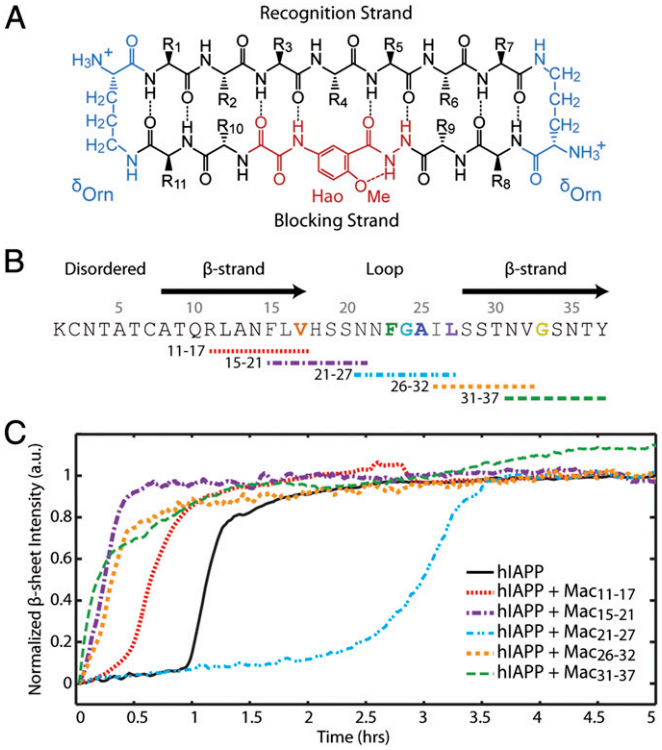

Fig. 2. Designed macrocycles and their effect on hIAPP aggregation. (*A*) General design of macrocyclic β-sheet peptides, including the "recognition" β-strand, the "blocking" β-strand (with the Hao unit in red), and the δ-linked ornithine turns (in blue). (*B*) Sequence of hIAPP labeled by its secondary structure. Sequences targeted by the recognition strand of the macrocycle are underlined. (*C*) Aggregation kinetics of hIAPP fibrils with and without macrocycles, monitored at 1,620 cm^{-1} and normalized to the equilibrated intensity.

species with parallel β-sheets at F23 will create such a feature. This conclusion is supported by an analysis of the kinetics. Fig. 1*G* shows the intensity of this peak monitored continuously as a function of time throughout aggregation relative to the intensity of the unlabeled β-sheet peak at 1,620 cm^{-1}. The F23 peak is present at the earliest times measureable, increases to a maximum during the lag phase, and then disappears at the same rate as the amyloid fibrils form. This rise and fall is the classic kinetic signature for an intermediate.

Similar to F23, samples labeled at G24, A25, and L27 all exhibit a coupled isotope peak during the lag phase (Fig. 1 *H–J*, boxes and arrows), indicating that the lag-phase intermediate has parallel β-sheet structure extending at least over residues 23–27 (FGAIL). Peak frequencies for both lag-phase and fibril spectra are summarized in Table S1 and additional lag-phase spectra are given in Fig. S4. F23 provides the clearest kinetic signature for the lag-phase β-sheet because F23 is completely uncoupled in the partially disordered loop and so does not appear as a defined peak in the fibril. The other residues remain coupled in the mature fibrils (Fig. S5 *A–C*) but are shifted to lower frequencies than in the oligomer, reflecting the change in structure from the oligomer to the fibril. Spectral overlap prevents a kinetic analysis of G24 and L27, but the A25 kinetics reveal that the spectral signature of the oligomer peaks at about the same time for A25 as for F23 (Fig. S6), which is consistent with the FGAIL intermediate forming in a single-step transition.

We do not know whether this β-sheet extends past the FGAIL sequence to include the flanking asparagine and serine residues because these amino acids are difficult to isotope label, but it does not extend as far as V17 or G33, neither of which is coupled during the lag phase (Fig. 1*C* and Fig. S4*B*); but V17 and G33 are coupled in the mature fibrils as expected (Fig.1*D* and Fig. S5*D*). It is possible that the early β-sheets are limited to residues 23–27, which would be consistent with early fragment studies showing that $hIAPP_{23–27}$ is the smallest fragment of hIAPP capable of forming amyloid fibrils (15). However, the $hIAPP_{22–27}$ fragment aggregates 40 times faster than $hIAPP_{23–27}$ and $hIAPP_{20–29}$ aggregates faster still, suggesting that the oligomeric β-sheets might extend beyond our labeled region to include the serines (15). Nonetheless, we know that the β-sheets must be small because, like typical random coil peptides, the unlabeled region of the spectra has only a minimal peak at 1,620 cm^{-1} (and does not extend to V17 or G33). Furthermore, transmission electron microscopy (TEM) images collected during the lag phase do not contain fibrils (Fig. 1*K* and Fig. S7*A*), in contrast to the images observed after aggregation is complete (Fig. S7*B*). Spherical deposits have been observed in other amyloid-forming systems and are often attributed to oligomeric species (31, 32).

The Use of Rationally Designed Macrocycles Confirms the Presence of the FGAIL Intermediate. To provide an independent test of our model, we studied the aggregation of hIAPP in the presence of rationally designed macrocyclic β-sheet peptides that are homologous to segments of hIAPP. The macrocycles comprise two anti-parallel β-strands connected by two δ-linked ornithines that mimic β-turns (Fig. 2*A*). One strand contains a heptapeptide sequence from hIAPP and the other strand contains an unnatural amino acid, Hao, which constrains the macrocycle to a β-sheet structure with four internal hydrogen bonds, but cannot form external hydrogen bonds. Thus, the heptapeptide strand of the macrocycle is designed to bind to amyloid β-sheets with a matching sequence, whereas the other strand prevents further elongation. Similar macrocycles have been used previously to study the aggregation of a τ-derived hexapeptide, amyloid-β, β2-microglobulin, and truncated α-synuclein (33, 34).

Five macrocycles were synthesized with heptapeptide sequences that span the length of hIAPP (Fig. 2*B*). Two macrocycles have sequences that overlap the N-terminal β-sheet of the fibrils ($Mac_{11–17}$ and $Mac_{15–21}$), two overlap the C-terminal sheet ($Mac_{26–32}$ and $Mac_{31–37}$), and one targets the FGAIL region under investigation ($Mac_{21–27}$). The sequences of the macrocycles are given in Fig. S8*A*. The macrocycles were mixed at equimolar concentrations with monomeric hIAPP and 2D IR spectra were collected continuously over the course of 5 h. Shown in Fig. 2*C* are kinetic traces plotting the intensity of the unlabeled β-sheet mode at ~1,620 cm^{-1}. The macrocycles do not have any spectral features in this range (Fig. S8 *B–F*) and so do not contribute significantly to the intensity measurements. The four macrocycles that overlap the fibril β-sheets accelerate hIAPP aggregation, reducing the lag time by 50% or more. The macrocycle that targets the FGAIL region ($Mac_{21–27}$) is markedly different. It slows amyloid formation, extending the lag time by 150%. TEM of equilibrated samples confirms the formation of amyloid fibrils (Fig. S7 *C* and *D*).

These results provide further evidence for an oligomeric intermediate. It is well established that the ends of sonicated amyloid fibrils will seed fibril growth by providing a β-strand to which hIAPP monomers template to form fibrils. Because these macrocycles are homologous with the β-sheets of the fibrils, accelerated kinetics are consistent with these macrocycles acting as seeds and templating formation of the N- and C-terminal β-sheets of the fibrils. In contrast, $Mac_{21–27}$ does not seed fibril formation because its target region is disordered in the fibril. Instead, $Mac_{21–27}$ inhibits fibril formation by stabilizing intermolecular interactions that must ultimately be disrupted to form the final fibril structure. This mode of inhibition is consistent with it recognizing the FGAIL β-sheet observed in the 2D IR experiments. The fact that $Mac_{21–27}$ is the only macrocycle that inhibits fibril growth is further evidence for formation of an intermediate containing β-structure in the FGAIL region.

The FGAIL Intermediate Is Predicted by Molecular Dynamics Simulation. To gain insight into the thermodynamics of hIAPP self-assembly, we use a bias-exchange metadynamics technique to calculate the free energy landscape for two hIAPP monomers (35, 36). We describe the surface with two order parameters, $Q_{8–16}$ and $Q_{27–35}$, where the subscripts refer to the hIAPP sequence. These order parameters are calculated by comparison with the N- and C-terminal β-sheets of the ssNMR fibril structure (4) and are designed to measure how closely the simulated structure matches the fibril (*SI Materials and Methods*). The resulting free energy landscape (Fig. 3) contains several intermediates labeled with Roman numerals. For each minimum, representative structures are presented with the FGAIL sequence colored in red. The map illustrates two possible minimum free energy pathways for the dimerization process: I → II → III → V and I → II → VI → V. The first intermediate encountered along either pathway is intermediate II, which contains a parallel β-sheet from residues 23–29, corresponding to the FGAILSS segment. Thus, the free energy landscape predicts that, as observed in experiments, the FGAIL region forms parallel β-sheets.

This landscape provides a physical rationale for the existence of the experimentally observed FGAIL intermediate. To progress from the intermediate (II) to the final structure (V), the FGAILSS β-sheet must break into a partially disordered loop. The loss of the FGAILSS structure is reflected in the high free energies of the intermediates III and VI, but the folded dimer with fully formed N- and C-terminal β-sheets (V) exhibits the lowest free energy. Thus, there is a free energy barrier associated with the breaking of the intermediate FGAILSS β-sheets into the partially disordered loop of the fibril, in agreement with experiment.

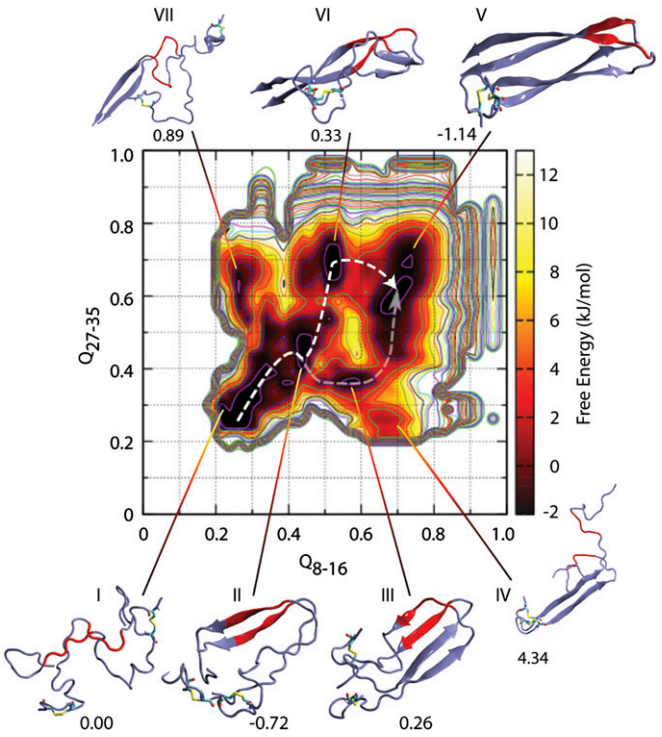

Fig. 3. Conformational free energy map for the dimerization of hIAPP in terms of order parameters $Q_{8–16}$ and $Q_{27–35}$. Contour lines are drawn every 2.5 kJ/mol. Representative dimer conformations for the seven local free energy minima are labeled I–VII, respectively, and the minimum free energy value in kJ/mol with respect to structure I is listed. Residues 23–27 are highlighted with red and the N-terminal disulfide bridge is represented with a stick model. Two minimum free energy paths of dimerization are highlighted by a white dashed arrow.

The metadynamics approach provides information on thermodynamics, not kinetics, and so experimental timescales are not relevant. For a dimer, the free energy minima all lie within ∼1.4 kJ/mol and thus all species will be populated at room temperature; however, we expect that intermediate II and the fibril will be further stabilized in simulations with additional peptides because free energy scales with the number of strands for small β-sheets (18).

Mutation Suggests That the FGAIL Oligomer Is on Pathway. The question remains as to whether these oligomers are on or off pathway. Kinetics experiments cannot distinguish between these two possibilities, nor can the macrocycle data because stabilizing the intermediate will slow fibril formation in either case. For this reason, we turn to the proline mutation I26P. Proline disrupts β-sheets and so I26P will prevent at least a portion of the FGAIL intermediate from forming. Destabilizing an on-pathway species will slow or prevent fibril formation (Fig. 4*A*), whereas destabilizing an off-pathway species should either not affect fibril formation or enhance it by closing a competing pathway (Fig. 4*B*). We find that the aggregation of I26P is >10 times slower than that of native hIAPP (Fig. 4*C* and Fig. S9 *A–C*), which is consistent with an on-pathway intermediate. To verify this conclusion, we performed two control experiments. First we confirmed that the altered kinetics are due to disruption of the intermediate rather than the fibril β-sheets by adding $Mac_{31–37}$. It seeds I26P fibril formation as it does with wild-type hIAPP, thus proving I26P can readily form fibrils and the proline mutation is not simply incompatible with the fibril structure. Second, we added $Mac_{21–27}$. Rather than inhibiting aggregation as it did with wild-type hIAPP, the macrocycle accelerates the aggregation of I26P. The reversed role is consistent with $Mac_{21–27}$ partially counteracting the effect of the proline and helping to template the formation of the on-pathway $hIAPP_{23–27}$ β-sheets. As a result, we conclude that the oligomeric species identified in this paper is likely an on-pathway intermediate in the fibril formation pathway.

Discussion and Conclusions

These experiments and simulations show that hIAPP fibril formation is a multistep process and that the hydrophobic sequence FGAIL plays a critical role in the aggregation mechanism under these conditions. It drives aggregation by forming a parallel β-sheet during the lag phase, but the FGAIL β-sheet is transient because the N- and C-terminal β-sheets of the fibril are ultimately favored by thermodynamics, for reasons that we discuss below. Our experiments and free energy calculations suggest that the lag phase during hIAPP aggregation under these conditions arises from a free energy barrier caused by breaking the intermolecular FGAIL β-sheets into the partially disordered loop of the fibril, thereby creating a free energy surface for amyloid formation that looks qualitatively like that shown in Fig. 5. The barrier may be very large, depending on the number of peptides contributing to the oligomeric β-sheet that must be disrupted. Once the turn is formed, aggregation into amyloid fibrils proceeds quickly. Macrocycles that match the fibril β-sheets circumvent this barrier whereas $Mac_{21–27}$ stabilizes the intermediate, increasing the barrier and thus lengthening the lag phase.

The data unambiguously indicate that the β-sheets have parallel, in-register strands across the FGAIL region. We cannot determine the size of these oligomers because both coupling and structural flexibility determine β-sheet frequencies, but the observed frequencies (1,585–1,588 cm^{-1}) are higher than those observed in the fibril and consistent with residues lying at the frayed edges of fibril β-sheets (30), implying a fair amount of structural disorder or smaller couplings than in typical flat β-sheets. Aromatic stacking interactions and hydrophobic collapse, often considered to be driving forces for fibril formation (37, 38), may drive the formation of the oligomers, although the

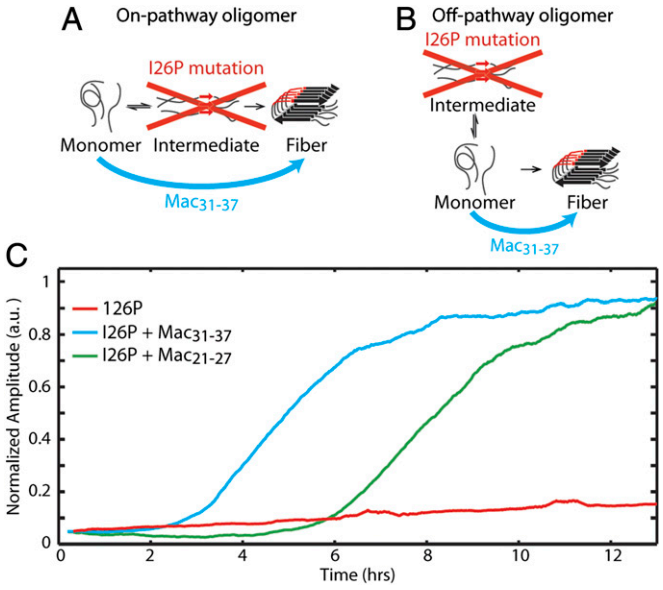

Fig. 4. Effect of I26P mutation on hIAPP aggregation. (*A* and *B*) Schematics showing the effects of proline mutation I26P on the aggregation of hIAPP, if the identified oligomers are (*A*) on pathway or (*B*) off pathway. (*C*) Aggregation kinetics of I26P fibrils, monitored at 1,620 cm^{-1}, alone (red) and with macrocycle Mac_{31-37} (cyan) or Mac_{21-27} (green).

amino acid composition of a peptide may not determine its aggregation propensity as much as the specific sequence (39).The fibrillation propensity of hIAPP, as calculated in the ZipperDB database compiled by Eisenberg and coworkers (39), predicts the FGAIL region as the most amyloidogenic region in the polypeptide (Fig. S1*B*). Crystal structures of short fragments of amyloidogenic proteins have highlighted the importance of steric zippers in which the side chains of stacked β-sheets interdigitate to convey stability (40). Likewise, hIAPP fibrils have interdigitated side chains (4). Interestingly, crystal structures of the NNFGAIL fragment do not form a steric zipper, but instead a tight and dry interface formed by the main chains (5). Thus, we postulate that the amyloidogenic nature of the FGAIL sequence drives the formation of intermediate β-sheets, which might exist as stacks of β-sheets, but the fibril is thermodynamically favorable because it has more extensive β-sheets and interdigitated side chains.

hIAPP can form at least two structures of fibrils, known as polymorphs (4). hIAPP fibrils prepared according to our methods have a backbone structure that closely matches that of the known polymorphs (29, 30), which differ in the packing of the side chains but not in the β-sheet secondary structure of the backbone. Because our 2D IR experiments do not probe side-chain packing, such polymorphs are not necessarily apparent in the spectra even though they are likely to be present. For the same reason, there may be multiple structures of the FGAIL intermediate to which we are insensitive, each leading to a different fibril polymorph. If so, the barriers associated with each polymorph must be similar because only a single sigmoidal rise is observed in the kinetic traces.

The intermediate appears to explain why mutations within and near the FGAIL region have a large impact on fibril formation. For example, rats, hamsters, and rabbits have multiple proline mutations within the 20–29 region that prevent the formation of the intermediate β-sheet, impeding or altogether inhibiting fibril formation (12). Nonnatural mutations, such as the inclusion of *N*-methylated amino acids (25) and the I26P mutant used in this work, further show that altering the FGAIL sequence dramatically affects the aggregation of hIAPP. In fact, peptide inhibitors that slow down or prevent hIAPP fibrillization often have mutations near residues 20–29 (23, 41, 42). Of course, mutations outside this region can play an important role by destabilizing the fibril itself (21, 22) and the aggregation pathway may be different in vivo or at different concentrations (43, 44). These results suggest that a strategy for preventing fibril formation and cytotoxic species could be to design inhibitors that disrupt the ordering of the FGAIL intermediate rather than targeting the fully formed fibrils.

In addition to helping explain the differences in aggregation propensity between species, the FGAIL intermediate also reconciles many of the original fragment studies (from which it was hypothesized that residues 20–29 formed the core β-sheets of the fibril) with the fibril structure (in which these residues are mostly disordered). We propose that the fragments highlight the importance of the intermediate in the aggregation mechanism whereas the full sequence is necessary to generate the actual fibril structure. This intermediate also sheds light on how structure influences amyloid kinetics. A common feature of all amyloid-forming proteins is the lag phase. Recent efforts to model amyloid formation with mass action expressions have highlighted the importance of primary and secondary nucleation (45–47). These models were generated from experiments on other proteins and under different conditions, but so far have not invoked stable intermediates or provided a structural mechanism that accounts for a lag phase. For hIAPP, the barrier created by the FGAIL intermediate impedes the proteins from adopting their final fold and so slows down the structural kinetics to create the lag phase. The barrier explains our original work on hIAPP kinetics in which we found that the N- and C-terminal β-sheets formed later than the loop (29), which we illustrate by the subsequent steps in Fig. 5. It is not known whether other amyloid-forming proteins have stable on-pathway intermediates, but fragments that form fibrils have been found in many other proteins, which may serve as a guide for uncovering other intermediate species.

Materials and Methods

A full description of methods is given in *SI Materials and Methods*. Briefly, hIAPP (48) and macrocyclic peptides (34) were synthesized and purified according to published methods. hIAPP was dissolved in deuterated hexafluoroisopropanol to fully disaggregate the peptides. Aggregation was initiated by reconstituting lyophilized samples in deuterated buffer (20 mM Tris, pH = 7.4). The final total peptide concentration was 0.5 mM for pure hIAPP samples, 1 mM for 75% isotope-diluted experiments, and 1 mM for

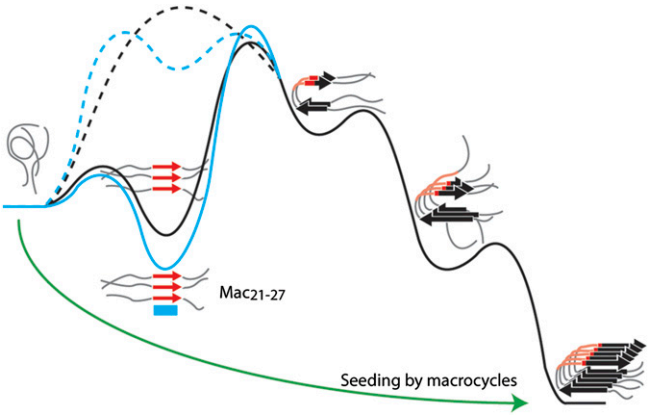

Fig. 5. Schematic energy landscape for hIAPP aggregation with schematic structures. Residues 23–27 are highlighted in red. Mac_{21-27} binds to the FGAIL intermediate, thereby stabilizing the intermediate (solid cyan) and increasing the free energy barrier, whereas the other four macrocycles circumvent the barrier by seeding fibril growth (green arrow). Proline mutations within the FGAIL sequence, such as I26P, inhibit aggregation by destabilizing the intermediate (dashed black line), which can still be induced to form by the addition of Mac_{21-27} (dashed cyan line).The subsequent steps are taken from our previous work on hIAPP aggregation (29).

samples containing equimolar hIAPP and macrocycle. Experiments with I26P were conducted at double the concentration of wild-type samples due to its significantly slowed kinetics. Two-dimensional IR spectra were collected as previously described (49). Bias-exchanged metadynamics simulations were conducted as described previously (36), using the ssNMR structure (4) as a reference.

ACKNOWLEDGMENTS. We thank Randall Massey at the University of Wisconsin Medical School Electron Microscope Facility for help with TEM. Support for this research was provided by the National Science Foundation (NSF) Graduate Research Fellowship Program Grant DGE-0718123 (to L.E.B.), National Institutes of Health (NIH) Grant DK79895 (to E.B.D., H.Q.T., and M.T.Z.), NSF Grant CHE-1112188 (to P.-N.C. and J.S.N.), NIH Grant 1R01DK088184 (to C.-C.C. and J.J.d.P.), and NIH Grant GM078114 (to P.C. and D.P.R.).

1. Chiti F, Dobson CM (2006) Protein misfolding, functional amyloid, and human disease. *Annu Rev Biochem* 75(1):333–366.
2. Butler AE, Janson J, Soeller WC, Butler PC (2003) Increased β-cell apoptosis prevents adaptive increase in β-cell mass in mouse model of type 2 diabetes: Evidence for role of islet amyloid formation rather than direct action of amyloid. *Diabetes* 52(9): 2304–2314.
3. Kayed R, et al. (2003) Common structure of soluble amyloid oligomers implies common mechanism of pathogenesis. *Science* 300(5618):486–489.
4. Luca S, Yau W-M, Leapman R, Tycko R (2007) Peptide conformation and supramolecular organization in amylin fibrils: Constraints from solid-state NMR. *Biochemistry* 46(47):13505–13522.
5. Wiltzius JJW, et al. (2008) Atomic structure of the cross-β spine of islet amyloid polypeptide (amylin). *Protein Sci* 17(9):1467–1474.
6. Ban T, Hamada D, Hasegawa K, Naiki H, Goto Y (2003) Direct observation of amyloid fibril growth monitored by thioflavin T fluorescence. *J Biol Chem* 278(19):16462–16465.
7. Measey TJ, Schweitzer-Stenner R (2011) Vibrational circular dichroism as a probe of fibrillogenesis: The origin of the anomalous intensity enhancement of amyloid-like fibrils. *J Am Chem Soc* 133(4):1066–1076.
8. Laganowsky A, et al. (2012) Atomic view of a toxic amyloid small oligomer. *Science* 335(6073):1228–1231.
9. Suzuki Y, et al. (2013) Resolution of oligomeric species during the aggregation of Aβ1-40 using (19)F NMR. *Biochemistry* 52(11):1903–1912.
10. Stroud JC, Liu C, Teng PK, Eisenberg D (2012) Toxic fibrillar oligomers of amyloid-β have cross-β structure. *Proc Natl Acad Sci USA* 109(20):7717–7722.
11. Kirkitadze MD, Condron MM, Teplow DB (2001) Identification and characterization of key kinetic intermediates in amyloid β-protein fibrillogenesis. *J Mol Biol* 312(5): 1103–1119.
12. Cao P, et al. (2013) Islet amyloid: From fundamental biophysics to mechanisms of cytotoxicity. *FEBS Lett* 587(8):1106–1118.
13. Betsholtz C, et al. (1989) Sequence divergence in a specific region of islet amyloid polypeptide (IAPP) explains differences in islet amyloid formation between species. *FEBS Lett* 251(1-2):261–264.
14. Westermark P, Engström U, Johnson KH, Westermark GT, Betsholtz C (1990) Islet amyloid polypeptide: Pinpointing amino acid residues linked to amyloid fibril formation. *Proc Natl Acad Sci USA* 87(13):5036–5040.
15. Tenidis K, et al. (2000) Identification of a penta- and hexapeptide of islet amyloid polypeptide (IAPP) with amyloidogenic and cytotoxic properties. *J Mol Biol* 295(4): 1055–1071.
16. Ashburn TT, Auger M, Lansbury PT (1992) The structural basis of pancreatic amyloid formation: Isotope-edited spectroscopy in the solid state. *J Am Chem Soc* 114(2): 790–791.
17. Glenner GG, Eanes ED, Wiley CA (1988) Amyloid fibrils formed from a segment of the pancreatic islet amyloid protein. *Biochem Biophys Res Commun* 155(2):608–614.
18. Wu C, Lei H, Duan Y (2004) Formation of partially ordered oligomers of amyloidogenic hexapeptide (NFGAIL) in aqueous solution observed in molecular dynamics simulations. *Biophys J* 87(5):3000–3009.
19. Mo Y, Lu Y, Wei G, Derreumaux P (2009) Structural diversity of the soluble trimers of the human amylin(20-29) peptide revealed by molecular dynamics simulations. *J Chem Phys* 130(12):125101.
20. Rivera E, Straub J, Thirumalai D (2009) Sequence and crowding effects in the aggregation of a 10-residue fragment derived from islet amyloid polypeptide. *Biophys J* 96(11):4552–4560.
21. Jaikaran ETAS, et al. (2001) Identification of a novel human islet amyloid polypeptide β-sheet domain and factors influencing fibrillogenesis. *J Mol Biol* 308(3):515–525.
22. Nilsson MR, Raleigh DP (1999) Analysis of amylin cleavage products provides new insights into the amyloidogenic region of human amylin. *J Mol Biol* 294(5):1375–1385.
23. Porat Y, Mazor Y, Efrat S, Gazit E (2004) Inhibition of islet amyloid polypeptide fibril formation: A potential role for heteroaromatic interactions. *Biochemistry* 43(45): 14454–14462.
24. Abedini A, Meng F, Raleigh DP (2007) A single-point mutation converts the highly amyloidogenic human islet amyloid polypeptide into a potent fibrillization inhibitor. *J Am Chem Soc* 129(37):11300–11301.
25. Yan L-M, Tatarek-Nossol M, Velkova A, Kazantzis A, Kapurniotu A (2006) Design of a mimic of nonamyloidogenic and bioactive human islet amyloid polypeptide (IAPP) as nanomolar affinity inhibitor of IAPP cytotoxic fibrillogenesis. *Proc Natl Acad Sci USA* 103(7):2046–2051.
26. Middleton CT, et al. (2012) Two-dimensional infrared spectroscopy reveals the complex behaviour of an amyloid fibril inhibitor. *Nat Chem* 4(5):355–360.
27. Kim YS, Liu L, Axelsen PH, Hochstrasser RM (2008) Two-dimensional infrared spectra of isotopically diluted amyloid fibrils from Abeta40. *Proc Natl Acad Sci USA* 105(22): 7720–7725.
28. Kim YS, Liu L, Axelsen PH, Hochstrasser RM (2009) 2D IR provides evidence for mobile water molecules in β-amyloid fibrils. *Proc Natl Acad Sci USA* 106(42):17751–17756.
29. Shim S-H, et al. (2009) Two-dimensional IR spectroscopy and isotope labeling defines the pathway of amyloid formation with residue-specific resolution. *Proc Natl Acad Sci USA* 106(16):6614–6619.
30. Wang L, et al. (2011) 2DIR spectroscopy of human amylin fibrils reflects stable β-sheet structure. *J Am Chem Soc* 133(40):16062–16071.
31. Hoshi M, et al. (2003) Spherical aggregates of β-amyloid (amylospheroid) show high neurotoxicity and activate tau protein kinase I/glycogen synthase kinase-3β. *Proc Natl Acad Sci USA* 100(11):6370–6375.
32. Papanikolopoulou K, et al. (2008) Formation of amyloid fibrils in vitro by human gammaD-crystallin and its isolated domains. *Mol Vis* 14:81–89.
33. Zheng J, et al. (2011) Macrocyclic β-sheet peptides that inhibit the aggregation of a tau-protein-derived hexapeptide. *J Am Chem Soc* 133(9):3144–3157.
34. Cheng P-N, Liu C, Zhao M, Eisenberg D, Nowick JS (2012) Amyloid β-sheet mimics that antagonize protein aggregation and reduce amyloid toxicity. *Nat Chem* 4(11):927–933.
35. Laio A, Parrinello M (2002) Escaping free-energy minima. *Proc Natl Acad Sci USA* 99(20):12562–12566.
36. Piana S, Laio A (2007) A bias-exchange approach to protein folding. *J Phys Chem B* 111(17):4553–4559.
37. Marshall KE, et al. (2011) Hydrophobic, aromatic, and electrostatic interactions play a central role in amyloid fibril formation and stability. *Biochemistry* 50(12):2061–2071.
38. Pawar AP, et al. (2005) Prediction of "aggregation-prone" and "aggregation-susceptible" regions in proteins associated with neurodegenerative diseases. *J Mol Biol* 350(2):379–392.
39. Goldschmidt L, Teng PK, Riek R, Eisenberg D (2010) Identifying the amylome, proteins capable of forming amyloid-like fibrils. *Proc Natl Acad Sci USA* 107(8):3487–3492.
40. Sawaya MR, et al. (2007) Atomic structures of amyloid cross-β spines reveal varied steric zippers. *Nature* 447(7143):453–457.
41. Sellin D, Yan L-M, Kapurniotu A, Winter R (2010) Suppression of IAPP fibrillation at anionic lipid membranes via IAPP-derived amyloid inhibitors and insulin. *Biophys Chem* 150(1-3):73–79.
42. Meng F, Raleigh DP, Abedini A (2010) Combination of kinetically selected inhibitors in trans leads to highly effective inhibition of amyloid formation. *J Am Chem Soc* 132(41):14340–14342.
43. Brender JR, Salamekh S, Ramamoorthy A (2012) Membrane disruption and early events in the aggregation of the diabetes related peptide IAPP from a molecular perspective. *Acc Chem Res* 45(3):454–462.
44. Williamson JA, Loria JP, Miranker AD (2009) Helix stabilization precedes aqueous and bilayer-catalyzed fiber formation in islet amyloid polypeptide. *J Mol Biol* 393(2):383–396.
45. Xue W-F, Homans SW, Radford SE (2008) Systematic analysis of nucleation-dependent polymerization reveals new insights into the mechanism of amyloid self-assembly. *Proc Natl Acad Sci USA* 105(26):8926–8931.
46. Knowles TPJ, et al. (2009) An analytical solution to the kinetics of breakable filament assembly. *Science* 326(5959):1533–1537.
47. Cohen SIA, et al. (2013) Proliferation of amyloid-β42 aggregates occurs through a secondary nucleation mechanism. *Proc Natl Acad Sci USA* 110(24):9758–9763.
48. Marek P, Woys AM, Sutton K, Zanni MT, Raleigh DP (2010) Efficient microwave-assisted synthesis of human islet amyloid polypeptide designed to facilitate the specific incorporation of labeled amino acids. *Org Lett* 12(21):4848–4851.
49. Middleton CT, Woys AM, Mukherjee SS, Zanni MT (2010) Residue-specific structural kinetics of proteins through the union of isotope labeling, mid-IR pulse shaping, and coherent 2D IR spectroscopy. *Methods* 52(1):12–22.